의학박사 학위논문

Preclinical SPECT imaging of choroidal neovascularization in mice using integrin-binding ^{99m}Tc-IDA-D-[c(RGDfK)]$_2$

2018 년 10 월

서울대학교 대학원

의학과 안과학전공

안 성 준

Preclinical SPECT imaging of choroidal neovascularization in mice using integrin-binding ^{99m}Tc-IDA-D-[c(RGDfK)]$_2$

지도교수 박 규 형

이 논문을 의학박사 학위논문으로 제출함

2018 년 10 월

서울대학교 대학원

의학과 안과학전공

안 성 준

안성준의 박사 학위논문을 인준함

2019 년 1 월

위 원 장 김 태 우 (인)

부 위 원 장 박 규 형 (인)

위 원 이 원 우 (인)

위 원 서 중 모 (인)

위 원 정 혜 원 (인)

Abstract

Preclinical SPECT imaging of choroidal neovascularization in mice using integrin-binding ^{99m}Tc-IDA-D-[c(RGDfK)]$_2$

Seong Joon Ahn
Department of Medicine (Ophthalmology)
The Graduate School
Seoul National University

Purpose: Integrin $\alpha_v\beta_3$, an adhesion molecule over-expressed in neovascular endothelial cells, is involved in ocular angiogenesis. Integrin $\alpha_v\beta_3$-binding arginine–glycine–aspartic acid (RGD) peptide has been used to target and visualize new vessels. We explored the use of integrin $\alpha_v\beta_3$-targeted RGD peptide (^{99m}Tc-IDA-D-[c(RGDfK)]$_2$) for *in vivo* molecular imaging of choroidal neovascularization (CNV).

Procedures: To induce CNV in animals, the right eyes of C57BL/6 mice were treated with retinal argon laser photocoagulation. CNV formation was confirmed on immunohistopathological examination of retinal and choroidal tissues. To explore the association of integrin with angiogenesis, integrin mRNA expression in the retinal and choroidal tissues was measured using real-time reverse transcriptase-polymerase chain reaction. For *in vivo* imaging, mice were intravenously injected with ^{99m}Tc-IDA-D-[c(RGDfK)]$_2$ and single-photon emission computed tomography (SPECT) images of ^{99m}Tc-IDA-D-[c(RGDfK)]$_2$ were obtained before laser induction (baseline) and at 1, 3, 7, and 14 days post-induction.

CNV-induced regional alterations were measured using radiotracer uptake.

Results: Immunohistopathological examination revealed that CNV lesions showed intense fluorescein isothiocyanate (FITC)-D-[c(RGDfK)]$_2$ immunofluorescence, in contrast to the normal retina and choroid. Retinal integrin mRNA expression peaked at Day 1 following CNV induction. On SPECT images using ^{99m}Tc-IDA-D-[c(RGDfK)]$_2$, the mean uptake of the radiotracer in eyes with CNV was significantly higher than in normal controls on Days 1–7 (all $p < 0.05$), with a peak at Day 3 representing the highest angiogenic activity. Our preclinical data demonstrated that ^{99m}Tc-IDA-D-[c(RGDfK)]$_2$ can detect CNV and its associated angiogenesis in an animal model of CNV.

Conclusions: SPECT imaging using an integrin $\alpha_v\beta_3$-targeted RGD peptide radiotracer may be a useful tool for *in vivo* imaging of CNV.

Keywords: age-related macular degeneration; choroidal neovascularization; molecular imaging; integrin; RGD peptide

Student Number: 2013-30551

Contents

List of Figures

Introduction

Age-related macular degeneration (AMD) is the leading cause of blindness among the elderly in developed countries (1, 2). Choroidal neovascularization (CNV), a key pathogenesis of exudative AMD, is one of the main causes of visual impairment in the disease (3-5). Structurally, CNV leads to retinal hemorrhage and exudates at the inner- or sub-retinal level, photoreceptor degeneration, and macular scar formation (5). However, the precise mechanisms of CNV development and the key molecules mediating the angiogenesis have not been fully determined. Furthermore, the current clinical imaging modalities of AMD, namely fluorescein angiography and optical coherence tomography (OCT), provide only structural information on disease status or developed CNV. A molecular imaging tool that can signal disease progression, or predict CNV formation or recurrence, has not been developed yet.

Among numerous modalities for treatment of exudative AMD, anti-vascular endothelial growth factor (VEGF) therapy has become the standard treatment to resolve CNV and improve vision (6). This success has validated angiogenesis as an important target for AMD treatment (7). However, recurrent CNV, which may lead to fibrosis and atrophy around the lesion, requires repeated intravitreal injections (8-10). Therefore, if a

molecular imaging tool could predict the development and recurrence of CNV before structural changes develop, early treatment and optimal visual outcomes could be achieved in patients with exudative AMD. During vascular remodeling and angiogenesis, several integrin families are expressed on the endothelial cells (11, 12). Among them, integrin $\alpha_v\beta_3$ is expressed preferentially on angiogenic blood vessels whereas its expression level in normal tissue is generally low (13, 14). Previous reports also showed that integrin $\alpha_v\beta_3$ is involved in ocular angiogenesis, which is a key pathological process of CNV formation (15, 16). Therefore, an integrin $\alpha_v\beta_3$-targeted probe is a potential diagnostic and therapeutic tool for CNV.

Arginine–glycine–aspartic acid (RGD) analogues, excellent targeting moieties for integrin $\alpha_v\beta_3$, have been shown to act as successful imaging agents for angiogenesis (17-19). We also recently developed a novel radiotracer, Tc-99m labeled RGD peptide analogue ([^{99m}Tc]IDA-D-[c(RGDfK)]$_2$), that showed excellent imaging potential in animal models of tumor angiogenesis and atherosclerosis (17-22).

The purpose of the present study was to develop a single-photon emission computed tomography (SPECT) tool for imaging of CNV using the integrin-targeted probe [^{99m}Tc]IDA-D-[c(RGDfK)]$_2$, and to validate it in preclinical setting. We also analyzed the correlation between *in vivo* uptake of [^{99m}Tc]IDA-D-[c(RGDfK)]$_2$ and *ex vivo* fluorescence staining of FITC-

D-[c(RGDfK)]$_2$ and the corresponding histopathological signatures.

Materials and Methods

2.1. Animals and materials

All research using a mouse model of CNV was approved by the Institutional Animal Care and Use Committee of the Seoul National University Hospital and adhered to the Association for Research in Vision and Ophthalmology statement for the Use of Animals in Ophthalmic and Vision Research. In total, 29 wild-type 6-week-old C57BL/6 male mice weighing 22 to 25 g were used for the experiments.

2.2. Induction of CNV

Procedures for inducing CNV were performed on C57BL/6 mice as described previously (23). A 512nm Argon laser system (Coherent PC-920 Argon Laser System; Coherent Medical Laser, Santa Clara, CA) were used. After intravenous anesthesia using a 1:1 mixture of 100 mg/ml ketamine and 20 mg/ml xylazine and pupillary dilatation with 5.0% phenylephrine and 0.8% tropicamide, mice received laser treatment in the right eye. The parameters of laser delivery were 100mW of power, 100ms of duration, and 100μm of spot size. For each eye, five spots of laser photocoagulation were made. To be a successful CNV lesion, a bubble should be observed immediately after laser treatment (24). When massive subretinal

hemorrhage occurred during the laser treatment, we stopped further treatment and excluded the animals from the experiment.

2.3. Histological and angiographic evaluation

Animals were euthanized and the eyes were enucleated and fixed in 4% paraformaldehyde. Serial sections of six eyes, enucleated at 2 weeks following CNV induction, were cut at 20 μm of thickness on a cryostat (HM550MP; Thermo Scientific, Waltham, Massachusetts, USA) at –20°C, and prepared for staining. Hematoxylin and eosin staining was performed for histological examination of the retina and choroid.

Ten eyes were prepared as choroidal flatmounts. For the flatmounts, mice were anesthetized at Day 7 or 14 and eyes were enucleated and fixed with 4% paraformaldehyde for 30 min at 4°C. The anterior segment and retina were removed from the eyecup, and four relaxing radial incisions were made. The remaining RPE–choroid–sclera complex was flatmounted and coverslipped. Flatmounts were examined with a scanning laser confocal microscope (LSM710; Carl Zeiss, Oberkochen, Germany).

FA was also performed using a commercial fundus camera and imaging system (Heidelberg Retina Angiography; Heidelberg Engineering, Heidelberg, Germany) following intraperitoneal injection of 0.2 ml of 2% fluorescein sodium at 1 week after laser photocoagulation. CNV was

confirmed with FA as a hyperfluorescent lesion with late-phase leakage (Fig. 1a).

2.4. Fluorescence staining of vessels in retinal and choroidal flatmounts using RGD peptides

The eyes were enucleated and fixed in 2% paraformaldehyde/PBS (phosphate buffered solution, pH 7.4) for 5 min. The retina and choroid were then isolated from eyeballs, and permeabilized with 0.5% Triton X-100, 5% fetal bovine serum, and 20% dimethyl sulfoxide (DMSO) in PBS for 3 h at room temperature (RT). For vessel staining, the retinas were incubated with BS-1 lectin-TRITC (Sigma-Aldrich) at 4°C for 4 days. The protected cyclic RGD-dimer peptide, NH_2-D-[c(R(Pdf)GD(tBu)fK)]$_2$, was provided by Bio Imaging Korea Co., Ltd. The precursor, NH_2-D-[c(RGDfK)]$_2$, was synthesized in our laboratory using a standard protocol based on a previously described method (20). Next, NH_2-D-[c(RGDfK)]$_2$ (10 nmol) was conjugated to 4 μg of fluorescein isothiocyanate (FITC; Thermo Fisher Scientific Korea Inc., Seoul, Korea) in 100 mM PBS (pH 7.5) with stirring for 1 h at RT. The FITC-labeled peptide was purified to >95% purity using C-18 reverse phase high-performance liquid chromatography (HPLC; Shimadzu Prominence, Kyoto, Japan) with a solvent mixture of acetonitrile/water/0.1% trifluoroacetic acid using a

gradient condition and confirmed using mass spectrometry (HP/Agilent 1100 series LC/MSD, Santa Clara, CA, USA). This FITC-labeled peptide, FITC-D-[c(RGDfK)]$_2$, was used for integrin $\alpha_v\beta_3$ targeting in CNV lesions.

Fluorescence staining with FITC-D-[c(RGDfK)]$_2$ was performed as follows: (1) the retinal and choroidal flatmounts were washed with PBS and incubated with FITC-D-[c(RGDfK)]$_2$ for 30 min; (2) the slides were washed with PBS several times, counterstained with 4',6-diamidino-2-phenylindole (DAPI), and mounted with ProLong Gold anti-fade reagent (Life Technologies, Carlsbad, CA, USA); (3) after staining, the flatmounts were mounted with the vitreous side up on glass slides and visualized on a confocal microscope (LSM710; Carl Zeiss, Oberkochen, Germany).

Additionally, we evaluated the specificity of FITC-D-[c(RGDfK)]$_2$ staining by using an excess of cRGD peptides. For this experiment, one mouse with identical laser-induced CNV in both eyes was sacrificed; one eye was stained with the staining method described above using 10 nM of FITC-D-[c(RGDfK)]$_2$ and the other was stained with the staining method described above plus a 2-h incubation with excess cRGD peptides (20-fold molar concentration of the FITC-conjugated cRGD dimer, i.e., 200 nM) prior to the fluorescence staining. In this staining, we also used an integrin $\alpha_v\beta_3$ antibody to investigate if the staining with the integrin $\alpha_v\beta_3$ antibody co-localized with that of the FITC-conjugated cRGD dimer.

2.5. RT-PCR for integrin expression in vitro

At baseline and at 1, 3, 7, and 14 days after CNV induction, four mice per time point were sacrificed and their eyeballs were enucleated. Total RNA was isolated from the retinal tissue using the RNeasy mini kit (Bio-Rad, Hercules, CA, USA). Reverse transcription was performed on 2 μg denatured RNA using the Superscript III First-strand Synthesis kit (Invitrogen). The relative abundance of integrins was analyzed using semi-quantitative PCR with BioMix (Bioline, London, UK) according to the manufacturer's protocol. Negative controls were performed without RT to confirm the absence of genomic DNA contamination. The reaction conditions of the above sequences were as follows: denaturation at 95°C for 5 min, extension at 58°C for 45 s, and annealing at 72°C for 60 s for 33 cycles. PCR products were separated on a 3% agarose gel by electrophoresis for 20 min at 150 V. PCR products were identified by their expected size.

2.6. ^{99m}Tc-IDA-D-[c(RGDfK)]$_2$ SPECT imaging of CNV lesions

The protected cyclic RGD-dimer peptide, NH2-D-[c(R(Pdf)GD(tBu)fK)]$_2$, was provided by Bio Imaging Korea Co., Ltd. and the radiotracer, [^{99m}Tc]IDA-D-[c(RGDfK)]$_2$, was synthesized as described previously (20-

22). [^{99m}Tc]pertechnetate was eluted on a daily basis from ^{99}Mo/^{99m}Tc-generator (Samyoung Unitech, Seoul, Korea).

[^{99m}Tc]IDA-D-[c(RGDfK)]$_2$ was prepared with radiochemical purity and specific activity greater than 99% and 55 GBq/μmol, respectively. After mice were placed in a prone position on the bed of an animal SPECT/CT scanner (NanoSPECT/CT; Bioscan Inc., Washington DC, USA) under anesthesia with 2% isoflurane, a high-resolution static scan of the mouse head was acquired in helical scanning mode in 24 projections after 30 min following intravenous injection of [^{99m}Tc]IDA-D-[c(RGDfK)]$_2$ (18.5 MBq in 200 μl) using a four-head scanner with 4 × 9 (1.4 mm) pinhole collimators. The energy window was set at 140 keV ± 15%. The SPECT image acquisition was followed using CT in the same position. From our previous work, [^{99m}Tc]IDA-D-[c(RGDfK)]$_2$ showed fast uptake at integrin-positive areas and rapid washout from integrin-negative organs; thus, there was an excellent target/background ratio in multiple organs, including brain, in both mouse and rat models at 30 min postinjection.[20-22] Therefore, we performed in vivo SPECT imaging of CNV in the eyes of C57BL/6 mice, using a previously performed protocol.(21, 22)

The analysis software HiSPECT (Version 1.0; Bioscan Inc., Poway, CA, USA) and In Vivo Scope (Version 1.43; Bioscan Inc., Poway, CA,

USA) were used for reconstruction and quantification, respectively. The accumulated radioactivity of [^{99m}Tc]IDA-D-[c(RGDfK)]$_2$ in eyes on the specified days was extracted from the images by drawing regions of interest (ROIs) using the 37 MBq radioactivity of [^{99m}Tc] sodium pertechnetate with 1.5 ml of saline in a 3-ml syringe as a reference source. The syringe was inserted into the opening in the appropriate quantification phantom. The count rates on all detectors should be approximately the same as when the syringe is centered in the field of view. The time per projection was calculated using the peak count rate (CPS). The minimum number of counts per projection was 50,000 counts and projection time was 50,000 counts divided by the peak count rate. SPECT images were used to measure [^{99m}Tc]IDA-D-[c(RGDfK)]$_2$ uptake in the laser-treated eye using the ROI method. The result was normalized to the injected radioactivity and expressed as the percentage of injected dose per cubic centimeter (%ID/cm^3).

2.7. SPECT imaging for evaluating the dose-response relationship and therapeutic response to anti-vascular endothelial growth factor treatment

An additional experiment involving the use of 1, 3, 6, and 15 laser spots for CNV induction in each eye was performed to compare the radiotracer uptake among the four groups of mice and consequently establish the dose-response relationship between the number of laser spots (also induced CNV)

and the signal intensity in SPECT.

Although there is no established treatment for complete regression of CNV in animal models, we administered an intravitreal injection of aflibercept (Eylea®; Bayer Healthcare) to the mice in the treated group; this treatment is commonly performed for patients with exudative age-related macular degeneration. Specifically, 1 μl (40 μg) of aflibercept was administered following CNV induction. In the other group (untreated group), CNV was induced and left untreated. Three mice from each group were subjected to SPECT imaging on Day 3.

2.8. Statistical analysis

The Wilcoxon signed rank test was used to assess differences among paired groups. Mann–Whitney test was used for comparison between independent groups. Continuous values are expressed as mean ± standard error (SE). P values less than 0.05 were considered statistically significant. Statistical analyses were performed by using SPSS version 18.0 (SPSS Inc., Chicago, Illinois, USA).

Results

3.1. Confirmation of CNV formation

CNV was induced by laser photocoagulation to disrupt Bruch's membrane, as noted in Fig. 1a. Immediately after laser induction, the formation of a vaporization bubble was noted. The formation of CNV was confirmed using fluorescein angiography (FA) (Fig. 1b). FA revealed hyperfluorescent spots with fluorescein leakage at the areas in which laser photocoagulation was performed, which is compatible with CNV. The spots with leakage were matched with those treated by laser induction.

Histopathologically, CNV eyes showed fibrovascular complex formation in the choroid and overlying retina with disruption of the retinal pigment epithelium (RPE) and the outer retina (Fig. 1c), which is also compatible with CNV. Immunofluorescence images of ICAM-2, integrin $\alpha_v\beta_3$, and DAPI co-staining revealed co-localization of ICAM-2 and integrin $\alpha_v\beta_3$ on the lesion (Fig. 2), also confirming the integrin $\alpha_v\beta_3$ expression on the CNV lesion.

3.2. Ex vivo *imaging of CNV and co-localization of integrins*

The FITC-labeled RGD peptide allowed the visualization of CNV at laser-treated areas (Fig. 3). Compared to the untreated fellow eye (Fig. 3a, left),

the CNV eye showed five lectin-positive, RGD-peptide-binding round spots (arrowheads), which topographically matched with the five laser-treated spots (Fig. 3a, right). These spots were co-stained with DAPI, lectin, and RGD peptide. A magnified image of one of the spots (square in Fig. 3a) better demonstrates the co-localization of the RGD-binding protein (integrin $\alpha_v\beta_3$) with lectin (Fig. 3b, top). In contrast, normal vessels in the retina, which are lectin-positive, were barely stained with FITC-labeled RGD peptide (Fig. 3b, bottom). This indicated that CNV could be imaged using an RGD peptide dimer-integrated probe as it selectively bound to CNV. Figure 4 shows the co-localization of RGD-binding protein and integrin $\alpha_v\beta_3$. However, the fluorescence of the FITC-labeled RGD peptide was remarkably reduced by excess cRGD.

3.3. Integrin expression

We examined integrin expression in the mouse retina over time after CNV induction by RT-PCR (Fig. 5). When normalized to the expression of the glyceraldehyde-3-phosphate dehydrogenase (*GAPDH*) gene, most integrins showed similar pattern of expression, i.e., an increase at the early stages (peak at Day 1) and a subsequent decrease over the following 2-week period, to the level similar to that at baseline (Fig. 5b). There was an increase in the expression of integrin α_V (1.48-fold) and β_3 (1.24-fold) at Day 1 after CNV

induction. The increase at Day 1 was statistically significant for α_V ($P < 0.05$). At Day 3, 7, and 14, there were no significant changes in expression of integrin α_V or β_3 compared to baseline.

3.4. In vivo *SPECT imaging of CNV*

Representative coronal, sagittal, and transverse planar SPECT-CT fusion images in laser-treated mice at 30 min after intravenous [^{99m}Tc]IDA-D-[c(RGDfK)]$_2$ injection are shown in Fig. 6a. Compared to untreated areas, the laser-treated mouse showed relatively intense radioactive signal. This figure shows quantitative changes in [^{99m}Tc]IDA-D-[c(RGDfK)]$_2$ uptake over time following CNV induction. In the laser-treated eyes, the radiotracer uptake showed an early increase up to Day 3 (when it peaked) and a subsequent decrease up to Day 14 (Fig. 6b). The increase from Day 1 through Day 7 compared to baseline was statistically significant (all $P < 0.05$). The radioactive uptake at Day 14 was decreased to a level similar to that at baseline.

By changing the number of laser spots used for CNV induction, the dose-response relationship between the number of spots and radioactivity uptake in SPECT was observed, as demonstrated in Fig. 6c. Radioactivity uptake showed an increasing trend with an increase in the number of laser spots, with significant differences among the subgroups divided according

to the number of laser spots ($P = 0.001$; ANOVA). More specifically, Fig. 7 shows the dose-response relationship in treated and untreated (control) eyes. The ratio of radioactive uptake in treated eyes to those in untreated eyes, which approximates the ratio of specific to nonspecific radioactive uptake, also showed a similar trend of increase, according to the number of laser spots.

Fig. 8 shows the comparisons of radioactivity uptake in SPECT imaging between anti-VEGF-treated and untreated mice. Treatment with intravitreal aflibercept injection showed a possible trend of decreased radioactivity uptake in the eyes with anti-VEGF treatment; however, the difference was not statistically significant ($P > 0.05$) and thus could not be confirmed.

Figure 1. Characterization of choroidal neovascularization (CNV) formation. (a) Fundus image obtained immediately after laser photocoagulation. Arrowheads indicate the laser-treated spots. Bubble formation is noted immediately after Bruch's membrane rupture (arrowheads). (b) Fluorescein angiography shows the CNV lesions with dye leakage from the laser-treated spots (arrowheads). (c) Hematoxylin and eosin (H&E)-stained cryosection (at 2 weeks following CNV induction) shows the fibrovascular complex and disruption of the outer retina, which is compatible with CNV.

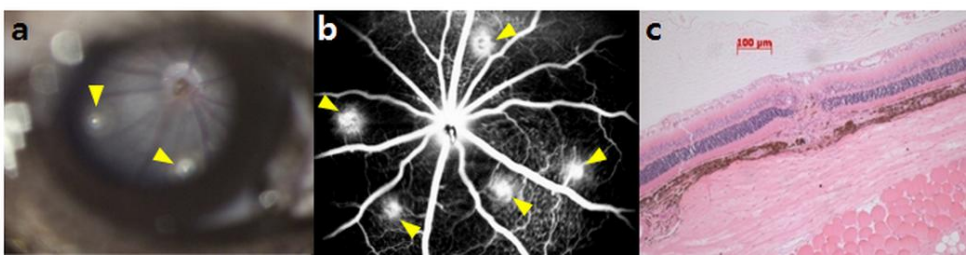

Figure 2. Representative images of ICAM-2, integrin $\alpha_v\beta_3$, and DAPI co-staining from frozen sections of laser–induced choroidal neovascularization (CNV) lesions. Integrin $\alpha_v\beta_3$ co-localizes with ICAM-2.

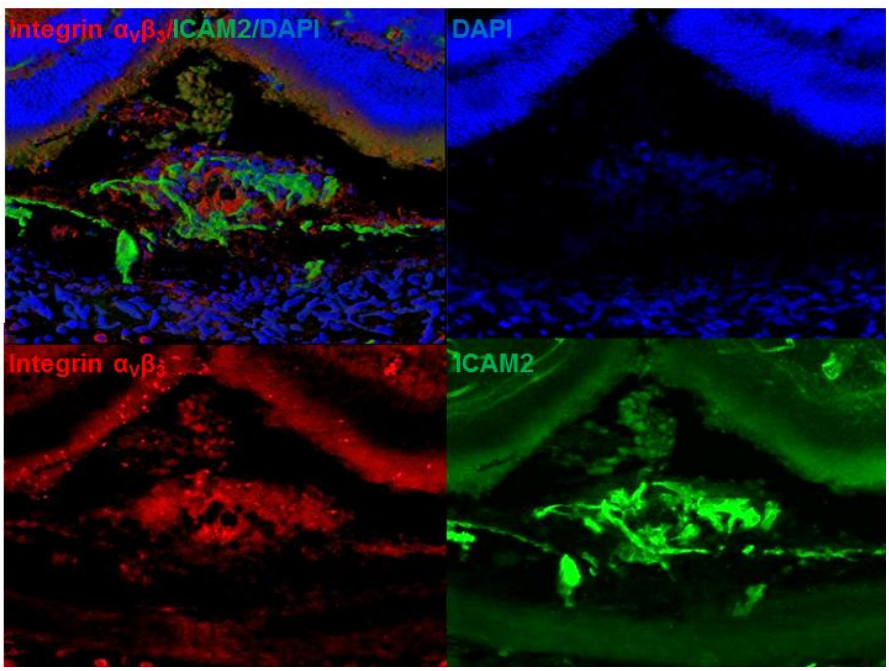

Figure 3. Choroidal flatmount immunofluorescence images obtained at 7 days after choroidal neovascularization (CNV) induction. (a) Compared to the untreated eye (left), the eye with CNV induction (right) shows hyperfluorescent spots, which correspond to the laser-treated areas (arrowheads). (b) More magnified images of CNV (square in a) show that the laser-treated lesion stained with FITC-labeled RGD peptide corresponded to that stained with lectin, indicating that CNV can be stained with an RGD-based probe. In the untreated retina (bottom), faint FITC-labeled RGD peptide immunofluorescence is observed along the retinal vessels.

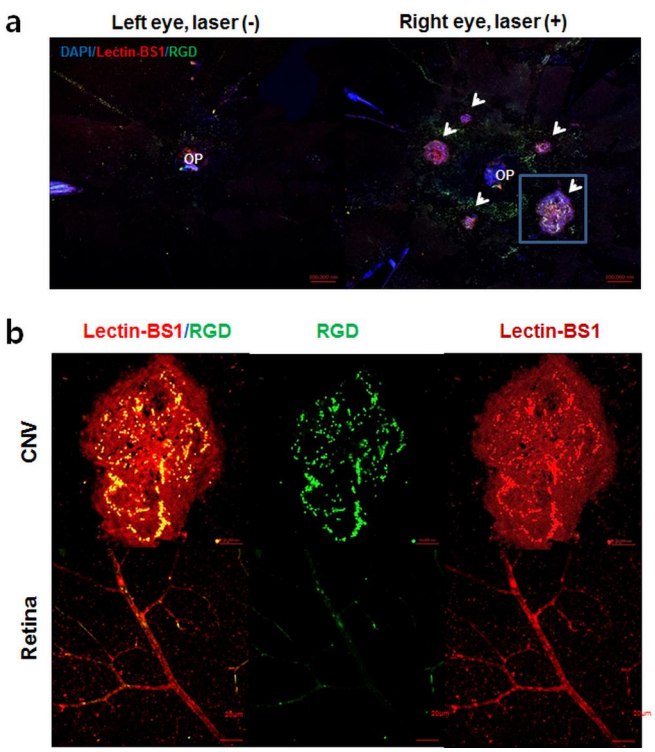

Figure 4. Fluorescence staining of choroidal flatmounts in a mouse treated with laser identically in both eyes. Both eyes were co-stained with DAPI, FITC-RGD, CD31, and integrin $\alpha_v\beta_3$ antibody; the left eye (**b**) was also incubated with excess cRGD before FITC-RGD staining.

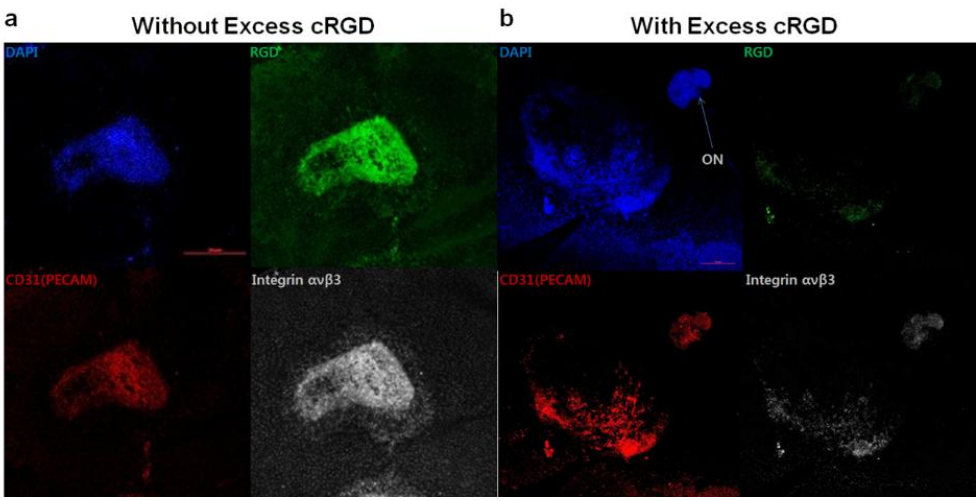

Figure 5. Reverse transcriptase polymerase chain reaction (RT-PCR, a) for integrin messenger RNA (mRNA) expression in the retina with laser-induced choroidal neovascularization (CNV) at 1, 3, 7, and 14 days. (b) Integrin expression data were normalized to the expression of the glyceraldehyde-3-phosphate dehydrogenase (*GAPDH*) gene. Upper bars indicate upper bound of 95% confidence interval. *P < 0.05

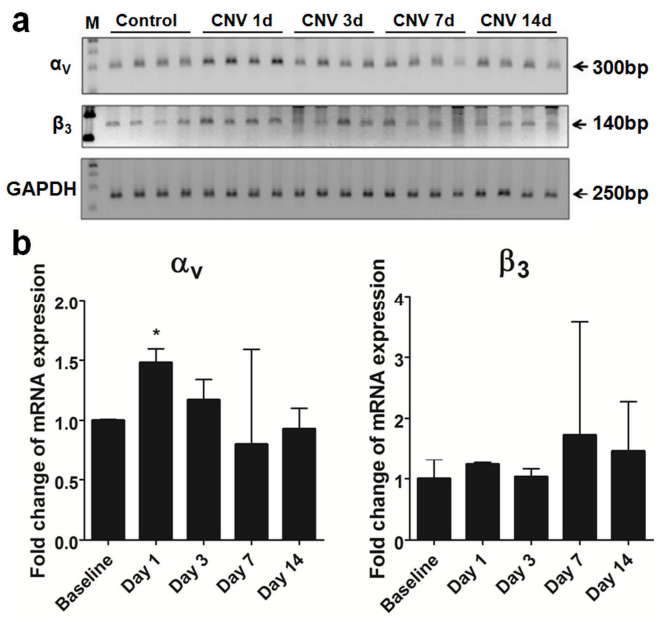

Figure 6. Serially obtained single photon emission computed tomography/computed tomography (SPECT/CT) images and quantification of angiogenic activity. (a) *In vivo* small animal SPECT/CT imaging using ^{99m}Tc-IDA-D-[c(RGDfK)]$_2$ and (b) quantitative analysis of *in vivo* ^{99m}Tc-IDA-D-[c(RGDfK)]$_2$ uptake in the choroidal neovascularization (CNV) model show increased radiotracer uptake at the early stage of CNV formation, which peaks at Day 3. (c) Radiotracer uptake shows an increasing trend with an increasing number of laser spots; there are significant differences among the subgroups, divided according to the number of laser spots. *P < 0.05

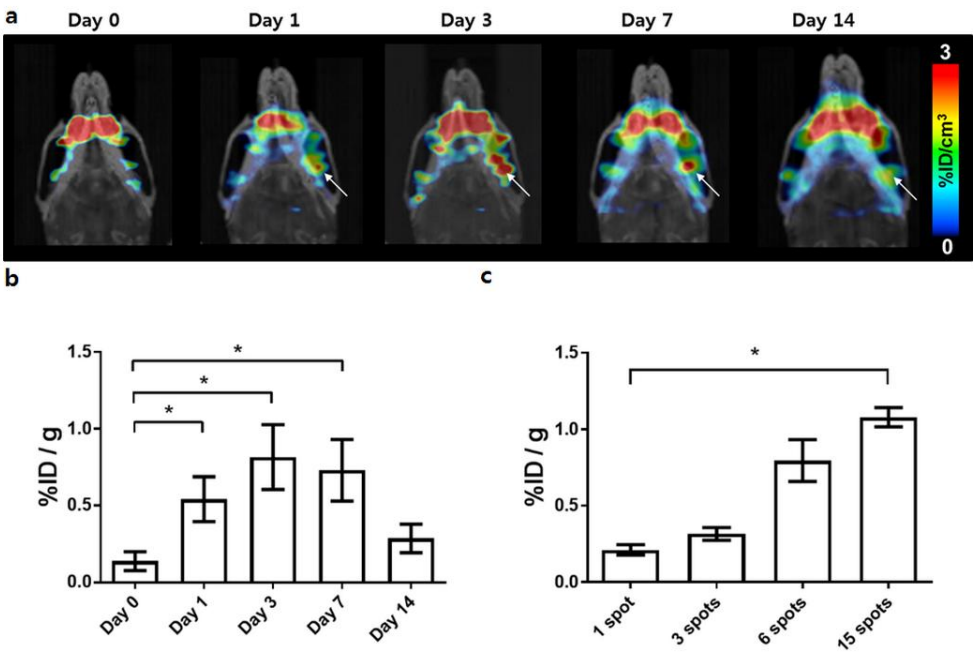

Figure 7. *In vivo* ^{99m}Tc-IDA-D-[c(RGDfK)]$_2$ uptake between laser-treated and control eyes (a) and the ratio of the uptake in treated eyes compared with that in control eyes (b). With an increasing number of laser spots, both radiotracer uptake in the treated eyes and the ratio of treated to control eyes increase.

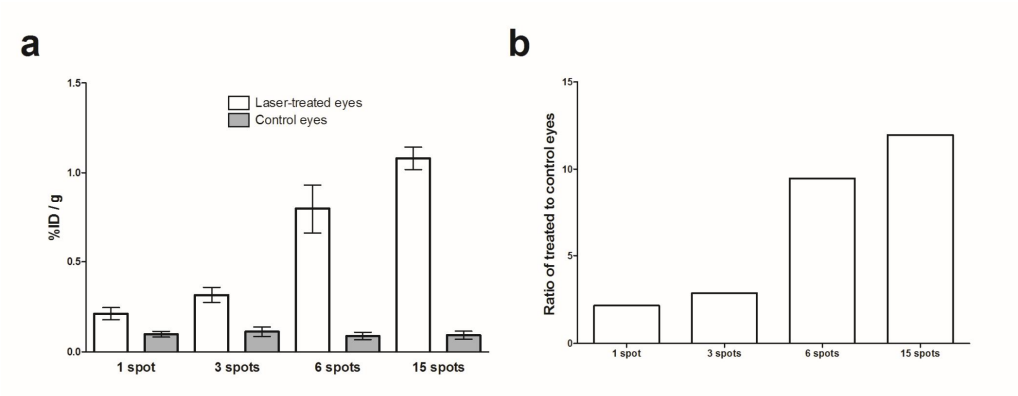

Figure 8. Comparison of *in vivo* ^{99m}Tc-IDA-D-[c(RGDfK)]$_2$ uptake between untreated mice and those treated with anti-vascular endothelial growth factor. The ratiotracer uptake showed a decreasing tendency in the treated group, although the difference between groups was not statistically significant and thus could not be confirmed.

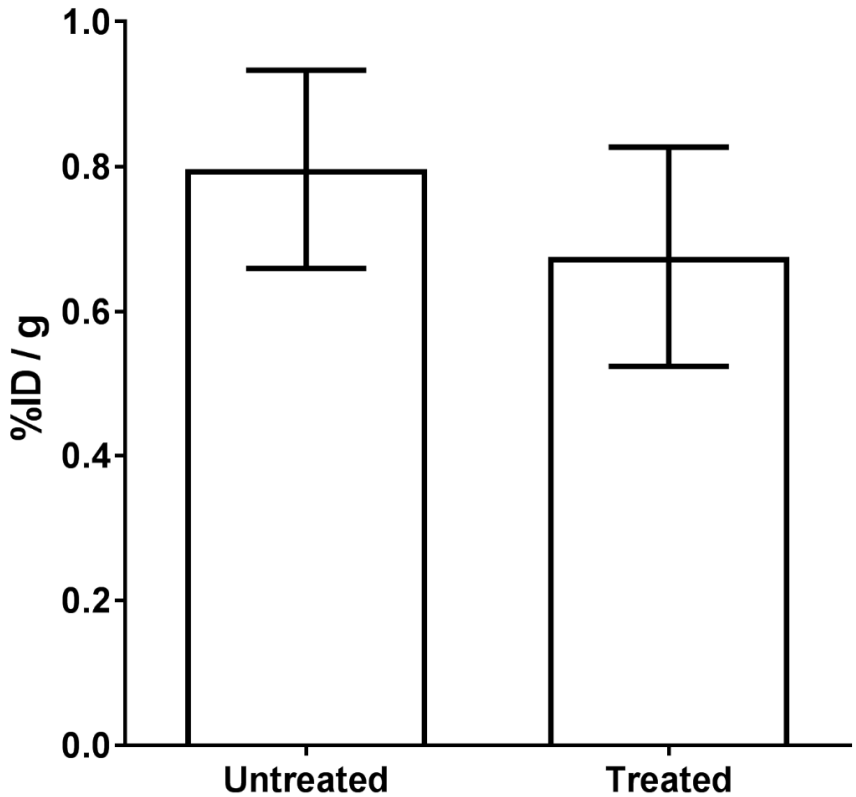

Discussion

By targeting integrin $\alpha_v\beta_3$ using a novel radioisotope-labeled RGD peptide, we obtained preclinical SPECT images in a mouse model of laser-induced CNV. This method enabled *in vivo* molecular imaging of CNV and quantification of angiogenic activity using a radioisotope.

Integrin $\alpha_v\beta_3$ is known to be up-regulated during the process of vascular remodeling and angiogenesis in eyes with AMD or diabetic retinopathy (12, 15, 16, 25, 26). Integrin $\alpha_v\beta_3$ is expressed on actively proliferating CNV membranes but not in normal retinal vessels (16), which was also observed in immunofluorescence images. Thus, the integrin appears to play a role in CNV angiogenesis and vascular remodeling, which should be investigated further. Using an integrin-binding RGD peptide, regardless of the role of integrin in angiogenesis, we developed a new method to visualize CNV and its activity by probing integrin $\alpha_v\beta_3$ functions *in vivo* as used for imaging angiogenesis in other organs (27).

However, it is remarkable that RT-PCR data showed discrepancy with the results obtained from the SPECT imaging. First, integrin mRNA expression was mildly increased, only statistically significantly so for the α_v subunit at Day 1 compared to baseline. We believe that the mRNA expression in the whole retina may not be significantly changed after CNV

induction while the area with CNV may show a remarkable change in integrin expression. Furthermore, the peak of mRNA expression, at Day 1, was different to the timing of the peak of RGD-based radiotracer uptake in the SPECT imaging, Day 3. The difference in the time of the peaks might be explained by the delay between mRNA and protein expression. Furthermore, the peak of radiotracer uptake in SPECT imaging also showed discrepancy with that in CNV formation. In previous studies, the peak of CNV formation was at 1 week after laser induction as the CNV lesion showed the largest area at that time (24). Therefore, the optimum time point to assess CNV formation after laser induction is typically at Day 7 (24), the time when our *ex vivo* CNV images were obtained. Previous results and ours portrayed a sequence of molecular events from mRNA expression of integrin induced by Bruch's membrane rupture to protein expression and subsequent development of phenotype (CNV formation), which occurs during 1 week following laser induction. The expression at Day 14, however, was similar to that at baseline. At that time, CNV is already formed. Therefore, this result is compatible with the previous findings that integrin expression is associated with the process of CNV formation. Based on the finding of peak time of integrin-targeting SPECT signal preceding the timing of CNV formation, this time discrepancy may allow early detection of CNV when applied clinically. Accordingly, the information on integrin activity using

the SPECT signal may facilitate early treatment of CNV and its recurrence before evident structural changes develop.

Our SPECT imaging findings can be correlated with the findings in a previous report describing in vivo OCT images of CNV in a mouse model.(28) On the basis of the morphological characteristics observed on OCT, three stages were suggested for the development of CNV following laser induction: early reaction phase, neovascular proliferation, and regression of the neovascular complex.(28) Neovascular proliferation occurs after initial reactions of the outer retina until Day 1 after laser-induced mechanical injury. On Day 5, well-delineated and organized subretinal material and fibrovascular tissue fills the empty space generated by laser-induced destruction. Therefore, the angiogenic activity for CNV development may be expected to be the maximum between Days 1 and 5; our finding of peak activity on Day 3, followed by a gradual decrease, supports these findings. Compatibility between the previous sequence of events for CNV formation and the sequence of angiogenic activity also supports the fact that the SPECT signal originates from the binding between the radiotracer and CNV, not from blood flow changes associated with thermal/mechanical injury following CNV induction, which are the maximum during the initial reaction phase (Days 0 and 1).

Our approach using a radioisotope-labeled RGD peptide has several

advantages over conventional imaging methods used for animal models of CNV. First, eyes with CNV induction can be serially followed using *in vivo* imaging without sacrificing the animal. Thus, time-dependent angiogenic activity and vascular remodeling can be monitored and compared within the animal. It may confer additional advantage for monitoring the therapeutic effect of potential drugs for CNV, as angiogenic activity may be compared before and after administration of the drug. Furthermore, even in patients with AMD, the imaging may be beneficial to visualize CNV in eyes with media opacity (e.g., cataract or subretinal hemorrhage), for which current imaging modalities such as FA and indocyanine green angiography are limited. When SPECT imaging is combined with current imaging modalities, it may identify retinal areas with angiogenic activity, which requires clinical attention for follow-up and treatment. Thus, this molecular imaging may be particularly useful for early detection of CNV and its recurrence. Also, our approach is different from previous integrin-targeted approaches for CNV detection in several ways, including specificity of targeting and the delivered material. The developed RGD dimer agent ^{99m}Tc-IDA-D-[c(RGDfK)]$_2$ showed more specific integrin-binding affinity than other reported RGD monomer-based agents (19, 29, 30), and thus provided better imaging performance for tumors and atherosclerotic plaques than the common monomeric RGD peptide probe (21).

However, our results regarding ex vivo imaging of CNV, presented in Suppl. Fig. 1 (see ESM), indicate that conducting FITC-D-[c(RGDfK)]$_2$ angiography may be more practical than conducting [^{99m}Tc]IDA-D-[c(RGDfK)]$_2$ SPECT imaging, as FITC angiography is already used in the clinic and FITC-D-[c(RGDfK)]$_2$ appears to provide images with better resolution than those of [^{99m}Tc]IDA-D-[c(RGDfK)]$_2$ SPECT. In this molecular imaging, we attempted to distinguish between signals from angiogenic activity and those from existing CNV. However, if FITC angiography is used, there would be several limitations to achieving this purpose. Scar tissues, the endstage of CNV, retain fluorescein; thus, both active and inactive CNV may be stained by FITC-D-[c(RGDfK)]$_2$. Accordingly, it may be impossible to discern active CNV (with angiogenic activity) from inactive CNV with scar tissues when angiography is performed using FITC-D-[c(RGDfK)]$_2$. Additionally, normal retina demonstrates fluorescence, regardless of intravenous injection of dye; this is known as fundus autofluorescence. Therefore, fluorescence detected using FITC-RGD angiography may be confounded by the presence of fundus autofluorescence. Accordingly, [^{99m}Tc]IDA-D-[c(RGDfK)]2 SPECT might be a more specific method to detect angiogenic activity in CNV; thus, our study used this method. However, FITC-D-[c(RGDfK)]$_2$ might also have potential for use in high-resolution imaging of the angiogenic activity of

CNV, and should be investigated further.

In addition to imaging, our findings might be applied to future development of targeted therapy of CNV using the novel RGD peptide. Prior studies used therapeutic chemicals as the delivered material, such as cationic nanoparticle coupled to an integrin $\alpha_v\beta_3$-targeted ligand (31) or sterically stabilized liposomes with RGD (32). Our results further suggest the potential of targeted therapy based on the RGD dimer agent, which requires further studies on its efficacy and systemic and ocular safety.

In the present study, it was possible to quantitatively measure radioactive uptake, which was the main purpose of the study; however, it was impossible to localize CNV in the images. The resolution of SPECT images was relatively low for localization of CNV in mouse eyes, which may be a limitation of SPECT as an imaging modality for CNV. However, in human eyes, of which the vitreous volume is approximately 400-fold larger than that of mouse eyes (33), the resolution of SPECT might be sufficient to localize CNV; notably, SPECT spatial resolution has also advanced. The potential of SPECT for the localization of CNV should be validated further in human eyes.

A limitation of this study was that maximum uptake and washout ratio was not obtained from laser-treated mouse eyes using serial SPECT imaging. Although we believe that this imaging protocol, in which SPECT images

were obtained at 30 min postinjection, can evaluate angiogenic activity of CNV, as in our previous works targeting angiogenesis, this must be confirmed or refined in future studies.

In summary, this study is a preclinical pilot study that provides evidence that a novel radioisotope-labeled RGD peptide can be used for *in vivo* molecular imaging of CNV. The SPECT imaging using the RGD-based probe may supplement current imaging modalities for detection of CNV, particularly for early detection of CNV development and its recurrence and for eyes with media opacity and subretinal hemorrhage. As our results were obtained using a small-animal model, our results should be confirmed in larger animals and finally in humans, which suggest the need for clinical trials. These results also encourage further investigations to develop integrin-targeted anti-angiogenic therapy using therapeutic radioisotopes.

References

1. Congdon N, O'Colmain B, Klaver CC, Klein R, Munoz B, Friedman DS, et al. Causes and prevalence of visual impairment among adults in the United States. Archives of ophthalmology. 2004;122(4):477-85.

2. Jager RD, Mieler WF, Miller JW. Age-related macular degeneration. The New England journal of medicine. 2008;358(24):2606-17.

3. Lee P, Wang CC, Adamis AP. Ocular neovascularization: an epidemiologic review. Survey of ophthalmology. 1998;43(3):245-69.

4. Zarbin MA, Casaroli-Marano RP, Rosenfeld PJ. Age-related macular degeneration: clinical findings, histopathology and imaging techniques. Developments in ophthalmology. 2014;53:1-32.

5. Green WR. Histopathology of age-related macular degeneration. Molecular vision. 1999;5:27.

6. Group CR, Martin DF, Maguire MG, Ying GS, Grunwald JE, Fine SL, et al. Ranibizumab and bevacizumab for neovascular age-related macular degeneration. The New England journal of medicine. 2011;364(20):1897-908.

7. Noel A, Jost M, Lambert V, Lecomte J, Rakic JM. Anti-angiogenic therapy of exudative age-related macular degeneration: current progress and emerging concepts. Trends in molecular medicine. 2007;13(8):345-52.

8. Brown DM, Michels M, Kaiser PK, Heier JS, Sy JP, Ianchulev T, et al. Ranibizumab versus verteporfin photodynamic therapy for neovascular age-related macular degeneration: Two-year results of the ANCHOR study. Ophthalmology. 2009;116(1):57-65 e5.

9. Rosenfeld PJ, Brown DM, Heier JS, Boyer DS, Kaiser PK, Chung CY, et al. Ranibizumab for neovascular age-related macular degeneration. The New England journal of medicine. 2006;355(14):1419-31.

10. Grunwald JE, Daniel E, Huang J, Ying GS, Maguire MG, Toth CA, et al. Risk of geographic atrophy in the comparison of age-related macular degeneration treatments trials. Ophthalmology. 2014;121(1):150-61.

11. Yancopoulos GD, Klagsbrun M, Folkman J. Vasculogenesis, angiogenesis, and growth factors: ephrins enter the fray at the border. Cell. 1998;93(5):661-4.

12. Brooks PC, Montgomery AM, Rosenfeld M, Reisfeld RA, Hu T, Klier G, et al. Integrin alpha v beta 3 antagonists promote tumor regression by inducing apoptosis of angiogenic blood vessels. Cell. 1994;79(7):1157-64.

13. Tucker GC. Alpha v integrin inhibitors and cancer therapy. Current opinion in investigational drugs. 2003;4(6):722-31.

14. Kumar CC, Armstrong L, Yin Z, Malkowski M, Maxwell E, Ling H, et al. Targeting integrins alpha v beta 3 and alpha v beta 5 for blocking

tumor-induced angiogenesis. Advances in experimental medicine and biology. 2000;476:169-80.

15. Luna J, Tobe T, Mousa SA, Reilly TM, Campochiaro PA. Antagonists of integrin alpha v beta 3 inhibit retinal neovascularization in a murine model. Laboratory investigation; a journal of technical methods and pathology. 1996;75(4):563-73.

16. Friedlander M, Theesfeld CL, Sugita M, Fruttiger M, Thomas MA, Chang S, et al. Involvement of integrins alpha v beta 3 and alpha v beta 5 in ocular neovascular diseases. Proceedings of the National Academy of Sciences of the United States of America. 1996;93(18):9764-9.

17. McDonald DM, Choyke PL. Imaging of angiogenesis: from microscope to clinic. Nature medicine. 2003;9(6):713-25.

18. Gaertner FC, Kessler H, Wester HJ, Schwaiger M, Beer AJ. Radiolabelled RGD peptides for imaging and therapy. European journal of nuclear medicine and molecular imaging. 2012;39 Suppl 1:S126-38.

19. Schottelius M, Laufer B, Kessler H, Wester HJ. Ligands for mapping alphavbeta3-integrin expression in vivo. Accounts of chemical research. 2009;42(7):969-80.

20. Lee BC, Moon BS, Kim JS, Jung JH, Park HS, Katzenellenbogen JA, et al. Synthesis and biological evaluation of RGD peptides with the $^{99m}Tc/^{188}Re$ chelated iminodiacetate core: highly enhanced uptake and

excretion kinetics of theranostics against tumor angiogenesis. RSC Adv. 2013(3):782-92.

21. Yoo JS, Lee J, Jung JH, Moon BS, Kim S, Lee BC, et al. SPECT/CT Imaging of High-Risk Atherosclerotic Plaques using Integrin-Binding RGD Dimer Peptides. Scientific reports. 2015;5:11752.

22. Lee MS, Park HS, Lee BC, Jung JH, Yoo JS, Kim SE. Identification of Angiogenesis Rich-Viable Myocardium using RGD Dimer based SPECT after Myocardial Infarction. Scientific reports. 2016;6:27520.

23. Reich SJ, Fosnot J, Kuroki A, Tang W, Yang X, Maguire AM, et al. Small interfering RNA (siRNA) targeting VEGF effectively inhibits ocular neovascularization in a mouse model. Molecular vision. 2003;9:210-6.

24. Lambert V, Lecomte J, Hansen S, Blacher S, Gonzalez ML, Struman I, et al. Laser-induced choroidal neovascularization model to study age-related macular degeneration in mice. Nature protocols. 2013;8(11):2197-211.

25. Brooks PC, Stromblad S, Klemke R, Visscher D, Sarkar FH, Cheresh DA. Antiintegrin alpha v beta 3 blocks human breast cancer growth and angiogenesis in human skin. The Journal of clinical investigation. 1995;96(4):1815-22.

26. Brooks PC, Clark RA, Cheresh DA. Requirement of vascular integrin alpha v beta 3 for angiogenesis. Science. 1994;264(5158):569-71.

27. Johnson LL, Schofield L, Donahay T, Bouchard M, Poppas A, Haubner R. Radiolabeled arginine-glycine-aspartic acid peptides to image angiogenesis in swine model of hibernating myocardium. JACC Cardiovascular imaging. 2008;1(4):500-10.

28. Giani A, Thanos A, Roh MI, Connolly E, Trichonas G, Kim I, et al. In vivo evaluation of laser-induced choroidal neovascularization using spectral-domain optical coherence tomography. Invest Ophthalmol Vis Sci. 2011;52(6):3880-7.

29. Haubner R, Wester HJ, Reuning U, Senekowitsch-Schmidtke R, Diefenbach B, Kessler H, et al. Radiolabeled alpha(v)beta3 integrin antagonists: a new class of tracers for tumor targeting. Journal of nuclear medicine : official publication, Society of Nuclear Medicine. 1999;40(6):1061-71.

30. Lee KH, Jung KH, Song SH, Kim DH, Lee BC, Sung HJ, et al. Radiolabeled RGD uptake and alphav integrin expression is enhanced in ischemic murine hindlimbs. Journal of nuclear medicine : official publication, Society of Nuclear Medicine. 2005;46(3):472-8.

31. Salehi-Had H, Roh MI, Giani A, Hisatomi T, Nakao S, Kim IK, et al. Utilizing targeted gene therapy with nanoparticles binding alpha v beta 3 for imaging and treating choroidal neovascularization. PloS one. 2011;6(4):e18864.

32. Ma L, Liu YL, Ma ZZ, Dou HL, Xu JH, Wang JC, et al. Targeted treatment of choroidal neovascularization using integrin-mediated sterically stabilized liposomes loaded with combretastatin A4. Journal of ocular pharmacology and therapeutics : the official journal of the Association for Ocular Pharmacology and Therapeutics. 2009;25(3):195-200.

33. Wallig MA, Haschek WM, Rousseaux CG, Bolon B (2018) Fundamentals of Toxicologic Pathology. 3rd ed.: Elsevier Inc.

국문초록

황반 변성 쥐모델에서 인테그린 결합 RGD 펩타이드를 이용한 맥락막 신생혈관 SPECT 이미징 전임상 연구

안성준

의학과 안과학

서울대학교 대학원

서론: 인테그린 $\alpha_v\beta_3$ 은 신생혈관에서 과발현되는 부착 분자 (adhesion molecule)로 안구내 신생혈관 과정과 연관되어 있음이 알려져있다. 인테그린 $\alpha_v\beta_3$ -결합 아르기닌-글리신-아스파라진산 (RGD) 펩티드는 신생혈관을 영상화 할 수 있을 것으로 사료된다. 이에 본 연구에서는 인테그린 $\alpha_v\beta_3$ -를 표적으로 하는 핵의학적 표지자를 부착한 RGD 펩티드 (^{99m}Tc-IDA-D-[c(RGDfK)]$_2$)를 이용하여 연령 관련 황반변성 동물 모델에서 분자 이미징을 시도하는 전임상 연구를 수행하고자 한다.

방법: 연령 관련 황반변성 동물 모델에서 맥락막 신생혈관을 유도하기 위해 C57Bl/6 쥐의 우안에 아르곤 레이저를 조사하였다. 맥락막 신생혈관 형성 여부는 면역형광 염색을 망막 및 맥락막 조직을 안구로부터 분리하여 확인하였다. 신생혈관 형성 (angiogenesis)와 인테그린의 관련성을 알아보고자, 인테그린 mRNA 발현 정도를 망막 및 맥락막 조직에서 실시간 역전사 중합효소반응을 이용하여 확인 및 정량화하였다. 이에 대한 분자적 in vivo 영상을 얻고자, 황반 변성 유도 쥐에 정맥 내 ^{99m}Tc-IDA-D-[c(RGDfK)]$_2$를 수행한 후, 단일광자방출컴퓨터단층촬

영 (single-photon emission computed tomography; SPECT)를 레이저 유도 전, 유도 후 1, 3, 7, 14일 째 시행하여 영상을 분석하였다. 황반 변성을 유도한 눈을 관심 영역으로 설정하여, radiotracer uptake를 측정하여, 정량화 하였다.

결과: 조직학적 검사에서 황반변성 유도 쥐의 망막에서 맥락막 신생혈관을 확인할 수 있었으며, 이는 fluorescein isothiocyanate (FITC)-D-[c(RGDfK)]$_2$ 면역형광에서도 확인할 수 있었다. 망막 내 인테그린 mRNA 발현은 레이저 조사 후 1일 째 정점에 달했으며, 이후 감소하는 양상이었다. SPECT 이미지에서는 레이저 유도를 하지 않은 반대안에 비해 레이저를 조사한 눈에서 유의하게 상승한 ratiotracer uptake count를 보였으며 레이저 후 3일째 가장 큰 활동성이 관찰되었다. 본 전임상 결과는 ^{99m}Tc-IDA-D-[c(RGDfK)]$_2$ 를 이용한 단일광자방출컴퓨터단층촬영이 황반변성 동물모델에서 맥락막 신생혈관을 확인하고, 관련된 혈관 형성 과정을 모니터링 할 수 있다는 점을 시사한다.

결론: 인테그린 $\alpha_v\beta_3$을 표적으로 하는 RGD 펩티드 표지자를 이용한 SPECT 이미징은 맥락막 신생혈관의 분자 이미징의 좋은 방법이 될 수 있다.

주요어 : 연령관련황반변성, 맥락막신생혈관, 분자이미징, 단일광자방출 컴퓨터단층촬영, 인테그린

학 번 : 2013-30551